THE JOURNAL OF BIOLOGICAL CHEMISTRY Vol. 278, No. 47, Issue of November 21, pp. 46506–46515, 2003

Printed in U.S.A.

Regulators of G Protein Signaling and Transient Activation of Signaling

EXPERIMENTAL AND COMPUTATIONAL ANALYSIS REVEALS NEGATIVE AND POSITIVE FEEDBACK CONTROLS ON G PROTEIN ACTIVITY*

Received for publication, August 1, 2003
Published, JBC Papers in Press, September 10, 2003, DOI 10.1074/jbc.M308432200

Nan Hao‡, Necmettin Yildirim§, Yuqi Wang‡, Timothy C. Elston§¶, and Henrik G. Dohlman‡‖

From the ‡Department of Biochemistry and Biophysics, University of North Carolina, Chapel Hill, North Carolina 27599-0812 and the §Department of Mathematics, University of North Carolina, Chapel Hill, North Carolina 27599-3250

Cellular responses to hormones and neurotransmitters are necessarily transient. The mating pheromone signal in yeast is typical. Signal initiation requires cell surface receptors, a G protein heterotrimer, and downstream effectors. Signal inactivation requires Sst2, a regulator of G protein signaling (RGS) protein that accelerates GTPase activity. We conducted a quantitative analysis of RGS and G protein expression and devised computational models that describe their activity *in vivo*. These results indicated that pheromone-dependent transcriptional induction of the RGS protein constitutes a negative feedback loop that leads to desensitization. Modeling also suggested the presence of a positive feedback loop leading to resensitization of the pathway. In confirmation of the model, we found that the RGS protein is ubiquitinated and degraded in response to pheromone stimulation. We identified and quantitated these positive and negative feedback loops, which account for the transient response to external signals observed *in vivo*.

One measure of our understanding of biological systems is our ability to predict their behavior in detail. One aspect of this endeavor is to model signal transduction events, defined here as the dynamic changes that occur within a cell in response to an external stimulus (1–3). Such models can help us to understand how small changes outside a cell produce strongly amplified changes within a cell, how graded signals are converted to all-or-none responses (4), or how activators of one pathway influence the function of a second pathway (5). A second goal, and the focus of this work, is to understand how transient external signals are prevented from being propagated indefinitely within the cell. Here we describe the molecular basis for signal activation, desensitization, and eventual resensitization of G proteins by receptors and RGS[1] proteins. The experimentally observed behavior is described mechanistically by computational modeling of the pathway.

For these studies we investigated the mating pheromone signaling pathway in yeast *Saccharomyces cerevisiae*. The yeast mating response is arguably the best characterized signal transduction pathway of any eukaryote, and it has long served as a prototype for hormone, neurotransmitter, and sensory response systems in humans (6). Disruption or activation of pathway components leads to highly specific changes that can be easily quantified. Finally, because it is a unicellular eukaryote, every cell in a population is genetically and phenotypically identical (all cells are "typical").

Mating in yeast is the fusion of **a** and α haploid cell types to form an **a**/α diploid. The events leading to fusion are initiated by specific pheromones: α-type cells secrete α-factor pheromone, which binds to a specific receptor (Ste2) on **a**-cells, while **a**-cells secrete **a**-factor that binds to receptors (Ste3) on α-cells. Upon pheromone binding to its receptor, the G protein α subunit (Gpa1) releases GDP, binds to GTP, and liberates the G protein $\beta\gamma$ subunits (Ste4/Ste18). Sustained signaling requires multiple effectors that bind to the dissociated Gα (7) and G$\beta\gamma$ components (8). These effectors go on to activate a mitogen-activated protein kinase cascade, leading to new gene transcription, morphological changes, cell division arrest, and ultimately cell fusion to form the **a**/α diploid (6). Following GTP hydrolysis, the G protein subunits reassociate and signaling stops (9).

One of the pheromone-induced genes encodes the prototype RGS protein Sst2. We have shown previously that Sst2 interacts genetically (10, 11) and physically (12) with Gpa1 and can accelerate its GTPase activity more than 40-fold (13). Mutants lacking *SST2* are ~100-fold more sensitive to pheromone (12, 14, 15). This pattern of induction and regulation of pheromone signaling suggests that Sst2 is part of a feedback inhibition loop that promotes desensitization. Although intuitively reasonable, this concept has never been tested explicitly. Moreover, while computational models of G protein activation and inactivation have been devised previously, they have not been rigorously tested *in vivo* due to a lack of information about expression levels or about specificity of coupling of receptors and G proteins (3, 16). Here we devise a detailed model that describes the behavior of cells treated with pheromone and demonstrate the predictive power of that model through experimentation.

EXPERIMENTAL PROCEDURES

Strains and Plasmids—Standard methods for the growth, maintenance, and transformation of yeast and bacteria and for the manipula-

* This work was supported by National Institutes of Health Grants GM55316 and GM59167 (to H. G. D.), by American Heart Association Fellowship 0225390U (to Y. W.), and by Defense Advanced Research Projects Agency Grant F30602-01-2-0579 (to T. C. E. and N. Y.). The costs of publication of this article were defrayed in part by the payment of page charges. This article must therefore be hereby marked "*advertisement*" in accordance with 18 U.S.C. Section 1734 solely to indicate this fact.

¶ To whom correspondence may be addressed. E-mail: telston@amath.unc.edu.

‖ To whom correspondence may be addressed. E-mail: hdohlman@med.unc.edu.

[1] The abbreviations used are: RGS, regulator of G protein signaling; SUMO, small ubiquitin-related modifier; GFP, green fluorescent protein; E1, ubiquitin-activating enzyme; E2, ubiquitin-conjugating enzyme; E3, ubiquitin ligase.

tion of DNA were used throughout (17). The yeast *S. cerevisiae* strains used in this study were BY4741 (*MAT***a** *leu2*Δ *met15*Δ *ura3*Δ) or BY4741-derived deletion mutants lacking *sst2*, *ubr1*, *ubc2/rad6*, *ubc4*, *ubc5*, *ubc7/qri8*, *ubc8*, *ubc10/pex4*, *ubc11*, *ubc12*, and *ubc13* (Research Genetics, Huntsville, AL). *UBC*-related gene deletion mutants not tested were *ubc1* (inviable), *ubc3/cdc34* (inviable), *ubc6* (unavailable), and *ubc9* (required for SUMOylation rather than ubiquitination).

Expression plasmids used in this study were those containing *STE2*, *GPA1*, *STE4*, *STE18*, and *SST2*. Each gene was amplified using flanking PCR primers that anneal 600 bp upstream or 600 bp downstream of the open reading frame. The PCR products were then subcloned by digestion with BamHI and either KpnI (*SST2* and *STE4*) or XhoI (*STE2*, *GPA1*, and *STE18*) (restriction site encoded by the PCR primers) and ligation to pRS316 (18). Other plasmids described previously are SST2-myc (12) expressed in pRS316-ADH (19) (plasmid pRS316-ADH-SST2-myc) and FUS1-GFP reporter (plasmid pDS30, from Daria Siekhaus, University of California, Berkeley) (20). Methods for purification of Sst2 (21) and Gpa1 (13) were described previously.

Signaling, Expression, Ubiquitination, and Degradation Assays—The pheromone-dependent transcription assays using the β-galactosidase (22) and green fluorescent protein (23) reporters have been described previously. For immunoblot detection, cell growth was stopped by the addition of 10 mM NaN_3 and transfer to an ice bath. To monitor the degradation of Sst2 over time, mid-log cell cultures were treated with cycloheximide (10 μg/ml in 0.1% ethanol, final concentrations) for up to 120 min before harvesting. Cells were washed and resuspended directly in boiling SDS-PAGE sample buffer (62.5 mM Tris-HCl, pH 6.8, 10% glycerol, 2% SDS, 1% 2-mercaptoethanol, 0.0005% bromphenol blue) for 10 min, subjected to glass bead homogenization, and clarified by microcentrifugation. Following SDS-polyacrylamide gel electrophoresis and transfer to nitrocellulose, the membrane was probed with antibodies to Ste2 at 1:2,000 (from James Konopka, State University of New York), Gpa1 at 1:1,000 (24), Ste4 at 1:2,000 (from Duane Jenness, University of Massachusetts), Ste18 at 1:100 (yN-16, Santa Cruz Biotechnology, Inc.), Sst2 at 1:2,000 (12), Myc (9E10) at 1:1,000 (25), or ubiquitin at 1:100 (Sigma). Immunoreactive species were visualized by enhanced chemiluminescence detection (Pierce) of horseradish peroxidase-conjugated anti-rabbit IgG (Bio-Rad) or anti-goat IgG (Santa Cruz Biotechnology, Inc.). Specificity of antibody detection was established using gene deletion mutants, diploid cells (which do not express the receptor, G protein, or RGS protein), or non-Myc-tagged *SST2* as negative controls.

Ubiquitinated Sst2 was enriched by immunoprecipitation prior to immunoblotting. Cells were grown to mid-log phase and either treated with 3 μM α-factor or with water for 1 h. Approximately 100 ml of cells at $A_{600\ nm} = 1$ were harvested and lysed at 4 °C in 600 μl of lysis buffer (25 mM Tris-HCl, pH 7.4, 200 mM NaCl, 15 mM EGTA, 15 mM $MgCl_2$, 0.1% Triton X-100, 10% glycerol, 1 mM NaN_3, 1 mM dithiothreitol, 10 mM *N*-ethylmaleimide, 5 mM phenylmethylsulfonyl fluoride, 1 μg/ml pepstatin, and 1 μg/ml leupeptin) with the use of acid-washed glass beads and 30-s pulses of vortexing, repeated six times. Samples were centrifuged for 10 min at 6,500 × *g*, and the resulting supernatant was removed and diluted to a final volume of 1 ml with wash buffer (the same as lysis buffer except there is no glycerol). Lysates were incubated with 40 μl of 9E10 anti-Myc antibodies for 90 min on ice. After clarification with a 10-min high speed microcentrifugation at 4 °C, protein-antibody complexes were precipitated for 1 h at 4 °C with 40 μl of a 50% slurry of protein G-Sepharose (Amersham Biosciences) equilibrated in wash buffer. Immunoprecipitates were collected by centrifugation at 2,000 × *g* for 30 s, and pellets were washed with wash buffer before final resuspension in 50 μl of 2× SDS-PAGE sample buffer.

Deterministic Modeling of Regulation by Sst2—To help elucidate the mechanism by which Sst2 regulates the pheromone response pathway, we constructed a simple mathematical model of the system. The variables in the model are the time-dependent concentrations of Ste4/Ste18 ([Gβγ]) and Sst2 ([RGS]). We assumed that the total concentration of Gβγ, $[G\beta\gamma]_T = [G\beta\gamma] + [G^{GDP}\alpha\beta\gamma]$, is constant in time. We also assumed that the rate-limiting step in the reformation of $G^{GDP}\alpha\beta\gamma$ after exposure to pheromone is the hydrolysis of GTP. Once hydrolysis occurs, $G^{GDP}\alpha$ and Gβγ rapidly combine to produce $G^{GDP}\alpha\beta\gamma$. The dynamics of [Gβγ] is governed by the ordinary differential equation.

$$\frac{d[G\beta\gamma]}{dt} = (k_1 + fk_1')([G\beta\gamma]_T - [G\beta\gamma]) - k_2[G^{GTP}\alpha] - k_3[RGS][G^{GTP}\alpha] \quad \text{(Eq. 1)}$$

The first term on the right-hand side of Equation 1 represents the rate at which free Gβγ is liberated from $G^{GDP}\alpha\beta\gamma$. The parameter k_1 is the rate constant for the process in the absence of pheromone, and k_1' is the pheromone-induced rate constant. The fraction of ligated receptors at pheromone concentration [*L*] is given by $f = [L]/(K + [L])$, where *K* is the effective dissociation constant for ligand binding. The second term on the right-hand side of Equation 1 represents the loss of free Gβγ by RGS-independent formation of $G^{GDP}\alpha\beta\gamma$. The reason this term does not explicitly depend on [Gβγ] is because of our assumption that, after exposure to pheromone, GTP hydrolysis is the rate-limiting step in the reformation of $G^{GDP}\alpha\beta\gamma$. The final term models the acceleration of this process by RGS (negative feedback). k_2 are k_3 are the corresponding rate constants for these two processes. By assuming that the total Gα concentration, $[G\alpha]_T = [G^{GDP}\alpha\beta\gamma] + [G^{GDP}\alpha] + [G^{GTP}\alpha]$, is constant in time and that $[G^{GDP}\alpha] \approx 0$, $[G^{GTP}\alpha]$ can be written in terms of [Gβγ] as follows: $[G^{GTP}\alpha] = [G\alpha]_T - [G\beta\gamma]_T + [G\beta\gamma]$. Making this substitution in Equation 1 produces the following equation.

$$\frac{d[G\beta\gamma]}{dt} = (k_1 + fk_1')([G\beta\gamma]_T - [G\beta\gamma]) - (k_2 + k_3[RGS])([G\alpha]_T - [G\beta\gamma]_T + [G\beta\gamma]) \quad \text{(Eq. 2)}$$

For the wild-type strain, we assumed that $[G\beta\gamma]_T = [G\alpha]_T$, and for the strain in which Gβ is doubly expressed, we assumed $[G\beta\gamma]_T$ is present at twice the wild-type level.

We assumed that the RGS concentration evolves according to the following equation.

$$\frac{d[RGS]}{dt} = k_4 + k_5[G\beta\gamma] - \delta[RGS] \quad \text{(Eq. 3)}$$

where k_4 is the constitutive rate of RGS production, k_5 is the pheromone-induced rate of RGS production, and δ is the degradation rate of RGS. While Equations 2 and 3 lack many biological details, it is shown under "Results" that this simple model provides insight into the signaling pathway. Equations 2 and 3 were solved numerically using MatLab. The pheromone-dependent transcriptional induction curves shown in Figs. 2*C* and 3*B* were produced from the relation $R = [G\beta\gamma]_{ss}/([G\beta\gamma]_{ss} + \kappa)$, where *R* is the response, $[G\beta\gamma]_{ss}$ is the steady-state value of [Gβγ], and κ is the value of [Gβγ] at which the response is half its maximum value. Equation 2 can be used to write *R* in terms of [*L*] and the steady-state RGS concentration $[RGS]_{ss}$. The result is given by Equation 10 where R_{min}, R_{max}, and *C* are defined as follows.

$$R_{min} = \frac{[G\beta\gamma]_T k_1 - (k_2 + k_3RGS)([G\alpha]_T - [G\beta\gamma]_T)}{\kappa(k_1 + (k_2 + k_3RGS)) + [G\beta\gamma]_T k_1 - (k_2 + k_3RGS)([G\alpha]_T - [G\beta\gamma]_T)} \quad \text{(Eq. 4)}$$

$$R_{max} = \frac{[G\beta\gamma]_T(k_1 + k_1') - (k_2 + k_3RGS)([G\alpha]_T - [G\beta\gamma]_T)}{(\kappa + [G\beta\gamma]_T)(k_1 + k_1') + (k_2 + k_3RGS)(\kappa - ([G\alpha]_T - [G\beta\gamma]_T))} \quad \text{(Eq. 5)}$$

$$C = \frac{\kappa(k_1 + (k_2 + k_3RGS)) + [G\beta\gamma]_T k_1 - (k_2 + k_3RGS)([G\alpha]_T - [G\beta\gamma]_T)}{(\kappa + [G\beta\gamma]_T)(k_1 + k_1') + (k_2 + k_3RGS)(\kappa - ([G\alpha]_T - [G\beta\gamma]_T))} \quad \text{(Eq. 6)}$$

The parameter values used to produce Figs. 2*C*, 3*B*, and 4 are $k_1 = 5.25 \times 10^{-5}\ min^{-1}$, $k_1' = 1.75\ min^{-1}$, $K = 2.0 \times 10^{-3}$ mM, $[L] = 3 \times 10^{-3}$ mM, $[G\beta\gamma]_T = 2 \times 10^{-4}$ mM, $k_2 = 3.5 \times 10^{-3}\ min^{-1}$, $k_3 = 3{,}500\ min^{-1}\ mM^{-1}$, $k_4 = 2.5 \times 10^{-6}\ mM\ min^{-1}$, $k_5 = 2.5 \times 10^{-2}\ min^{-1}$, $\delta = 5 \times 10^{-2}\ min^{-1}$, and $\kappa = 2.0$ mM.

To simplify the model further, we made the reasonable assumption that changes in free Gβγ occur on a much shorter time scale than changes in RGS expression. That is, we assumed that [Gβγ] is in equilibrium with respect to the current RGS expression level. Mathematically this means that the time derivative in Equation 2 is equal to zero. Solving the resulting equation for [Gβγ] and substituting the result into Equation 3 produces the following equation.

$$\frac{d[RGS]}{dt} = k_4 + \frac{k_5[G\beta\gamma]_T(k_1 + fk_1')}{fk_1' + k_1 + k_2 + k_3[RGS]} - \delta[RGS] = k_4 + \frac{S}{K_{nf} + [RGS]} - \delta[RGS] \quad \text{(Eq. 7)}$$

where $S = k_5[G\beta\gamma]_T(k_1 + fk_1')/k_3$ and $K_{nf} = (fk_1' + k_1 + k_2)/k_3$, and we made the simplifying assumption that $[G\beta\gamma]_T = [G\alpha]_T$. In the above

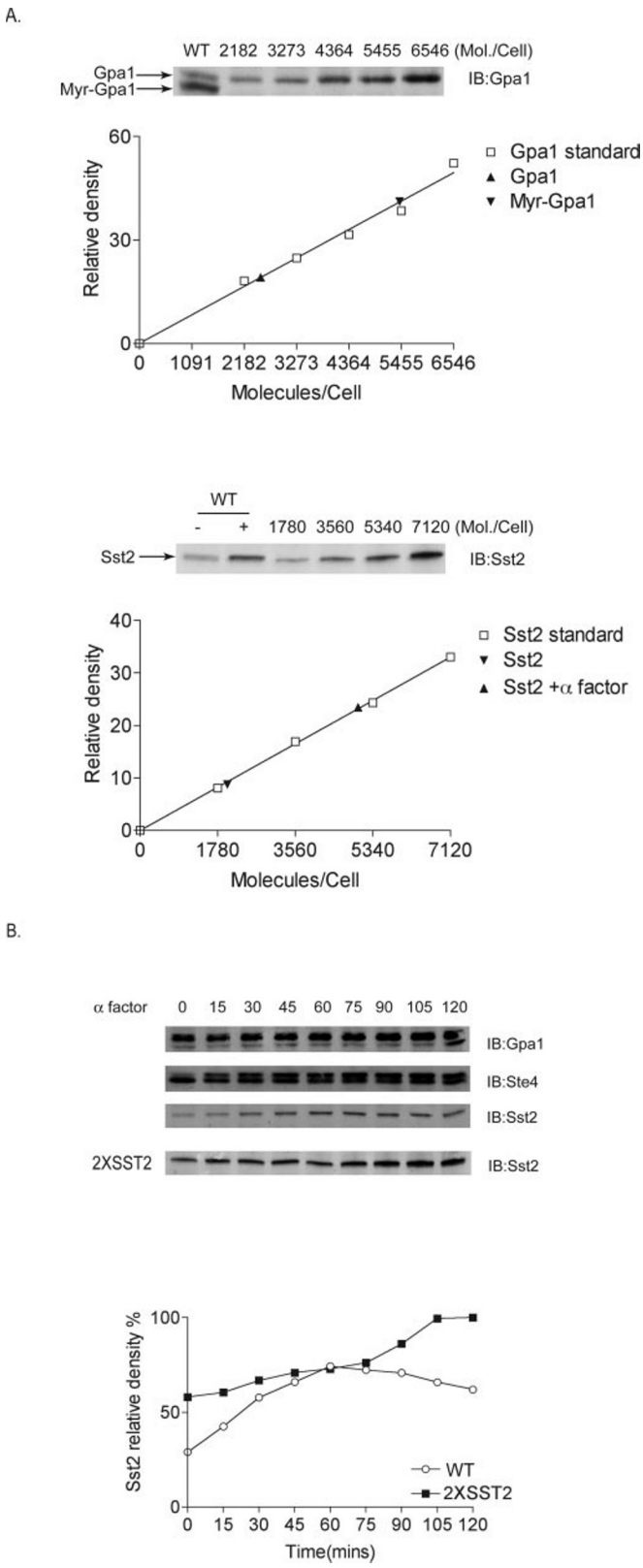

FIG. 1. **Time course of RGS and G protein induction after pheromone stimulation.** *A*, to determine the levels of expression of Sst2 and Gpa1 in yeast, known amounts of purified recombinant protein (*standard*) were mixed with whole-cell lysates from *gpa1*Δ and *sst2*Δ mutants, respectively, resolved by 7.5% SDS-PAGE and immunoblotting, and probed with anti-Gpa1 and anti-Sst2 antibodies as indicated (*IB*). To estimate the relative protein expression the bands were analyzed by densitometric scanning. Calculated expression levels of endogenous Gpa1 and Sst2 with (+) and without (−) 1-h treatment with 3 μM α-factor are summarized in Table I. Note that a portion of endogenous Gpa1 and none of the *Escherichia coli*-expressed Gpa1 is myristoylated (*Myr-Gpa1*) as reported previously (24, 44). *B*, whole-cell extracts were prepared from wild-type (BY4741) cells transformed with a single copy plasmid (pRS316) containing genomic *SST2* (2xSST2) or no insert and treated with 3 μM α-factor for the indicated times. Samples were resolved by 7.5% SDS-PAGE and immunoblotting and probed using anti-Gpa1, anti-Ste4, or anti-Sst2 polyclonal antiserum as indicated (*IB*). The *upper* Ste4 band corresponds to the phosphorylated form of the protein and is induced by pheromone (28). The specificity of each antibody was confirmed using gene deletion or diploid cells lacking the indicated gene product (not shown). To estimate the difference in protein expression the Sst2 band was analyzed by densitometric scanning (*bottom panel*). The data shown are representative of two independent experiments. *WT*, wild type; *IB*, immunoblot; *Mol.*, molecules.

TABLE I
Protein expression

Numbers in parentheses are maximum values (after pheromone treatment).

Protein	Number/cell	Source
Receptor (Ste2)	8,000	Ref. 27
Gα (Gpa1)	8,000 (12,000)	Experimental measurement
Gβ (Ste4)	8,000	Inferred
Gγ (Ste18)	8,000	Inferred
RGS (Sst2)	2,000 (5,000)	Experimental measurement

equation, the negative effect of RGS is clear. The maximum response in the absence of RGS is S/K_{nf}. As [RGS] increases, the production rate returns to k_4.

Stochastic Modeling of Sst2/RGS Inhibition—Whereas deterministic models describe the average behavior of a number of individual cells, stochastic models describe the diverse behavior of many individual cells as well as the random changes within a single cell. To illustrate that pheromone-induced Sst2 degradation through ubiquitination is sufficient to explain the experimental results obtained for the 2xSST2 strain, we modified Equation 7 in the following way.

$$\frac{d[\mathrm{RGS}]}{dt} = k_4 + \frac{S}{K_{nf} + [\mathrm{RGS}]} - \delta[\mathrm{RGS}](1 + [L]g([\mathrm{RGS}])) + \mathrm{Noise} \quad \text{(Eq. 8)}$$

The function g models the effect of pheromone-induced ubiquitination and increases the degradation rate. We assumed that RGS inhibits its own degradation, which would be the case if free Gβγ initiated the pathway leading to RGS ubiquitination, and took g to have the following form.

$$g([\mathrm{RGS}]) = \frac{g_{max}[\mathrm{RGS}]}{K_{RGS} + [\mathrm{RGS}]^4} \quad \text{(Eq. 9)}$$

where g_{max} is the maximum value of g, and K_{RGS} determines where g reaches half its maximum value. Finally we added a noise term in Equation 8 to model fluctuations in the concentration due to the stochastic nature of chemical reactions. In general, the strength of the noise depends on the biochemical reactions in the signaling pathway (26). However, for simplicity we modeled this term as Gaussian white noise of strength D. Equation 8 was solved numerically using an Euler method, and 10,000 realizations of the process were used to produce the results shown in Fig. 6, *B* and *C*. The parameter values used in these figures are $k_4 = 0.02$, $S = 0.36$, $K_{nf} = 0.09$, $K_{RGS} = 0.35$, $[L]\, g_{max} = 0.9$, $\delta = 0.2$, and $D = 0.0001$.

RESULTS

Our goal in this work was to understand how external signals produce responses within the cell. Our focus was on G protein activation, desensitization, and eventual resensitization by receptors and RGS proteins. Since an accurate model of any biological system requires knowledge of the identity and quantity of its components, we began by determining the amount of the RGS (Sst2) and Gα (Gpa1) present in the cell. The Gβγ subunits Ste4 and Ste18 were presumed to be expressed at levels equal to Gpa1 since G protein subunits assemble in a 1:1:1 stoichiometry, and Ste4 and Ste18 do not bind to any other Gα in yeast. Receptor expression was determined by radioligand binding measurements to be ~8,000/cell (27).

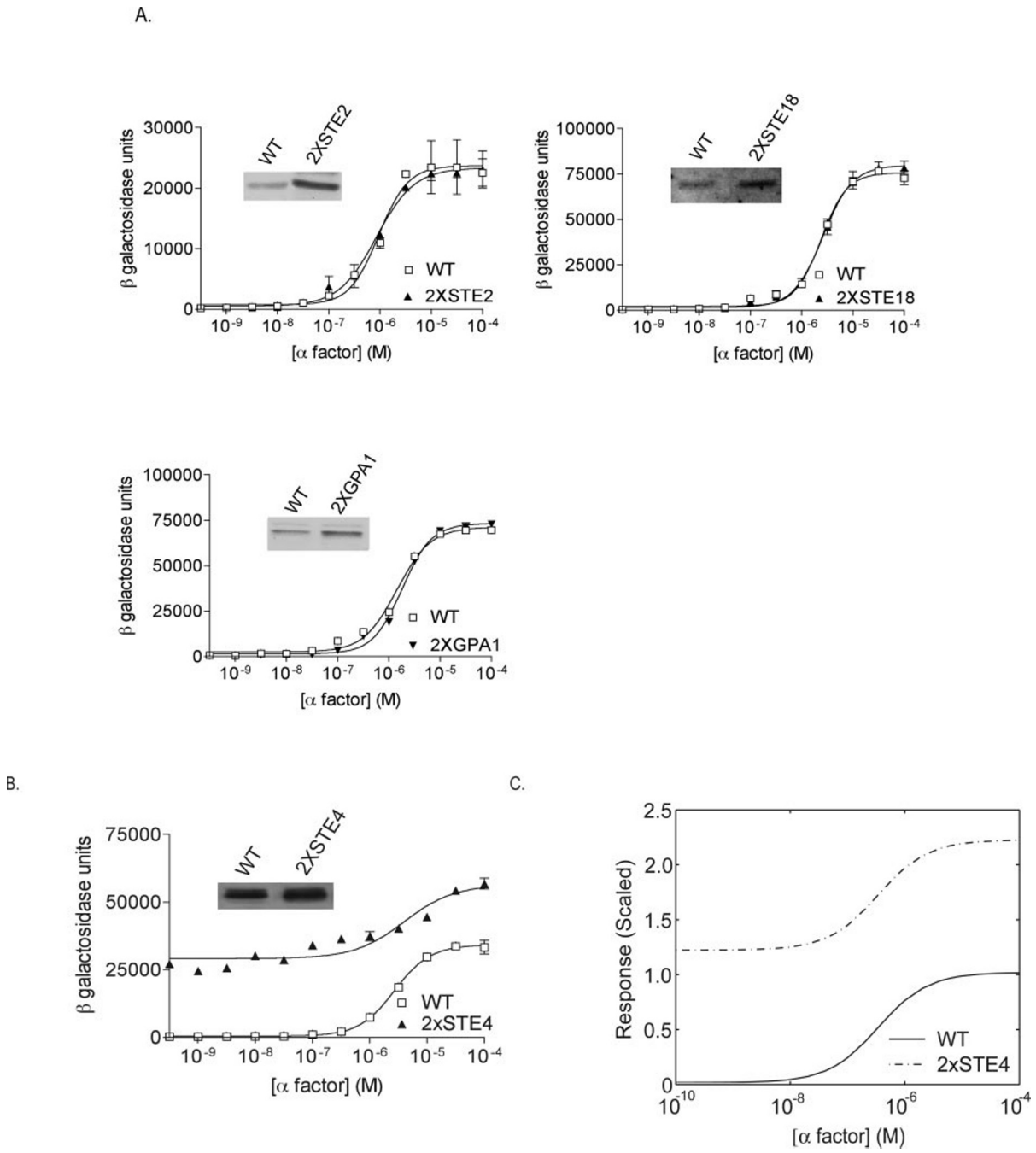

FIG. 2. **Double expression of Ste4 activates the mating pathway.** Pheromone-dependent transcriptional induction was measured following transformation of wild-type cells with a single copy plasmid (pRS316) containing genomic *STE2* (*2xSTE2*), *GPA1* (*2xGPA1*), or *STE18* (*2xSTE18*) (*A*) or *STE4* (*2xSTE4*) (*B*) and co-transformation with a pheromone-responsive *FUS1* promoter-*lacZ* reporter (pRS423-FUS1-lacZ). Cells were then treated with the indicated concentrations of α-factor for 90 min, and the resulting β-galactosidase activity was measured spectrofluorometrically. Activity is given in arbitrary units. To avoid selection for spontaneous sterile mutations the *STE4*-overexpressing cells were co-transformed with *GPA1* under control of the *GAL1/10* promoter (pRS315-GAL-GPA1) and maintained in galactose medium until the final inoculation into dextrose medium prior to performing the experiment. *Insets*, to confirm double expression of each gene product, the same cells were lysed and analyzed by immunoblotting with anti-Ste2, anti-Gpa1, anti-Ste4, or anti-Ste18 polyclonal antibodies. The data shown are representative of at least two independent experiments performed in triplicate. *C*, predicted pheromone-dependent transcriptional induction for the wild-type (*WT*) (*solid line*) and 2xSTE4 (*dot-dashed line*) strains. The model accurately captures the increased activity over the entire range of pheromone concentrations observed above for doubled expression of *STE4*. The response is scaled relative to the maximum response in wild-type cells (response = 1). Details of the model and the parameter values used to produce these and subsequent results are given under "Experimental Procedures."

To measure expression of Sst2 and Gpa1, we performed quantitative immunoblotting of whole-cell extracts. Cells in mid-log phase were harvested, lysed directly in SDS-PAGE sample buffer, and resolved by gel electrophoresis and immunoblotting. Absolute expression levels were determined using standards in which known quantities of purified recombinant Sst2 or Gpa1 were mixed with lysates from *sst2*Δ or *gpa1*Δ mutants, respectively. These data reveal that each cell contained ~8,000 copies of Gpa1, equal to the number of receptors, and ~2,000 copies of Sst2 (Fig. 1*A* and Table I).

Since the genes that encode *GPA1* and *SST2* are induced upon pheromone stimulation, we also monitored the expression levels of the encoded proteins over the course of a 2-h treatment with α-factor. The relative expression of each protein was again

determined by immunoblotting (Fig. 1*B*). These data reveal that Sst2 was induced 2.5-fold after 1 h of treatment and then declined slightly during the remainder of the experiment. Gpa1 expression was increased by ~50% and remained elevated even after 2 h. Ste4 expression was not altered, although it does undergo a mobility shift as a result of pheromone-dependent phosphorylation (28). These results are summarized in Table I.

We also examined whether perturbations in the expression of each signaling component would alter the pheromone response. Cells expressing normal amounts of Sst2, receptor, and all three G protein subunits were compared with cells engineered to express double ("2x") the normal amount of each component (Figs. 2 and 3). For this purpose, genomic copies of *STE2*, *GPA1*, *SST2*, *STE4*, and *STE18* were subcloned into a centromere-based shuttle vector and transformed into wild-type cells. An *sst2*Δ mutant was also tested since that would provide information about pathway activation in the absence of feedback inhibition and GTPase acceleration. Other deletions lead to permanent activation of the pathway (*gpa1*Δ) or a complete loss of responsiveness (*ste2*Δ, *ste4*Δ, and *ste18*Δ) and were not tested (6). Changes in protein expression were confirmed in each case by immunoblotting using polyclonal antibodies against Ste2, Gpa1, Ste4, and Sst2. Alterations in pheromone sensitivity were measured using a reporter transcription assay comprised of a pheromone-responsive promoter (from *FUS1*) fused to *lacZ* (β-galactosidase). This particular assay was chosen because it is sensitive, quantitative, and highly specific for Gpa1 signaling (22). We chose not to use fluorescence-based measures of G protein dissociation because they require modifications or fusions that might alter G protein stability, localization, or activity (29).

As shown in Fig. 2, 2-fold overexpression of the receptor, G protein α-subunit, and Gγ subunit had no effect on pheromone sensitivity. In contrast, overexpression of Gβ produced a dramatic increase in activity over the entire range of pheromone concentrations. Basal activity (no pheromone added) was also elevated so that it was nearly equivalent to wild-type cells treated with a maximally effective dose of pheromone. Thus 2-fold overexpression of Gβ is sufficient to fully activate the pathway. This is consistent with the model that Gβγ is necessary and sufficient for pathway activation and that Gβ is the limiting component of the Gβγ heterodimer complex (30). Twofold overexpression of *SST2* led to a reduction in the maximum response by 27% (Fig. 3*A*). Deletion of *SST2* did not alter the maximum response but rather resulted in a 100-fold decrease in the concentration of α-factor necessary to achieve 50% of the maximum agonist response (EC_{50}) (Fig. 3*A*). These data reveal that, while loss of *SST2* affected potency (a decrease in EC_{50}), overexpression of *SST2* caused a decrease in efficacy or maximum response.

Having established for each component the expression levels and functional consequences of altered expression (Figs. 2 and 3), we devised a simple mathematical model to describe pathway activation and inactivation with a set of two coupled ordinary differential equations. A detailed description of the modeling is provided under "Experimental Procedures" and is shown schematically in Fig. 4*A*. The model assumes that Gγ is produced in excess of Gβ (but Gβ is limiting so final expression levels are equal) and that receptor and Gα are present in equal amounts and are always associated so that individually changing the concentration level of Gγ, receptor, and Gα does not affect the model. These assumptions were consistent with data shown in Fig. 2 for the double expression of Ste18, Ste2, and Gpa1. Thus the model only considers Gβγ and the RGS protein. Free Gβγ activates the intracellular signal leading to new gene expression, and the RGS protein has a negative effect on the pathway by increasing the rate at which Gβγ recombines with $G^{GDP}\alpha$. The model produces several predictions that can be compared with the experimental results presented above. Typical time series generated by the model for release of free Ste4/Ste18 ([Gβγ]) and the expression of Sst2 ([RGS]) are shown in Fig. 4*B*. The model predicts a sharp initial increase of free Gβγ in response to pheromone followed by a slow decrease as the Sst2 concentration begins to rise. The initial slow rise in Sst2 expression is in good qualitative agreement with data shown in Fig. 1*B* for the wild-type (*WT*) strain. However, the model cannot reproduce the slow decline in Sst2 levels seen at later times (see below). The model can be used to derive an expression for response *R* of the signaling pathway as a function of pheromone concentration [*L*]. The general form of this expression is as follows.

$$R = \frac{R_{min}C + R_{max}[L]}{C + [L]} \qquad \text{(Eq. 10)}$$

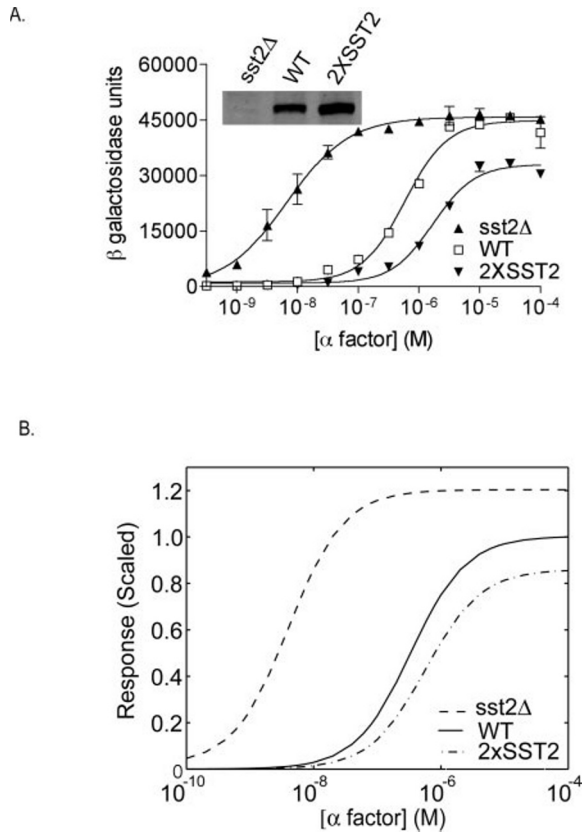

FIG. 3. **Double expression of Sst2 attenuates the response to pheromone.** *A*, pheromone-dependent transcriptional induction was measured following transformation of wild-type cells with a single copy plasmid (pRS316) containing genomic *SST2* (2xSST2), transformation of wild-type cells with the same plasmid containing no insert (*WT*), or transformation of an *sst2*Δ mutant with plasmid containing no insert (*sst2*Δ). The same cells were co-transformed with a pheromone-responsive *FUS1* promoter-*lacZ* reporter. Cells were then treated with the indicated concentrations of α-factor for 90 min, and the resulting β-galactosidase activity was measured spectrofluorometrically. *Inset*, to confirm expression of Sst2, the same cells were lysed and analyzed by immunoblotting with anti-Sst2 polyclonal antibodies. The data shown are representative of at least two independent experiments performed in triplicate. *B*, predicted pheromone-dependent transcriptional induction for the three strains shown in *A*. The model captures the decrease in EC_{50} seen in the *sst2*Δ strain (*dashed line*) relative to the wild-type strain (*solid line*). However, it cannot fully account for the decrease in the maximal response seen in the 2xSST2 strain (*dot-dashed line*) without also producing an artificial increase in the maximal response of the *sst2*Δ strain. The response is scaled relative to the maximum response in wild-type cells (response = 1).

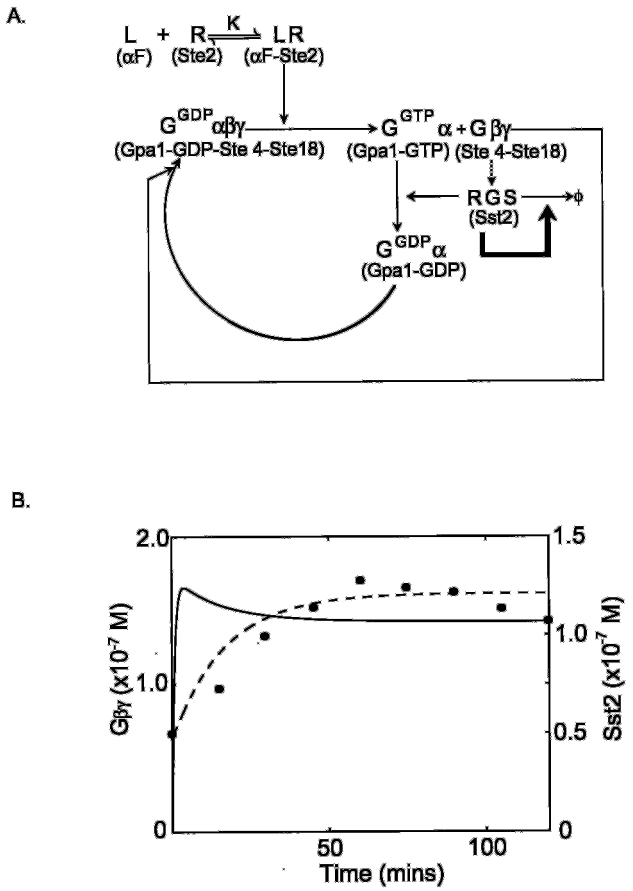

FIG. 4. **Pathway regulation by RGS and Gβγ proteins.** *A*, upon binding of the ligand (*L*) α-factor (*αF*) to its receptor (*R*, Ste2), the G protein α subunit (Gpa1) releases GDP, binds to GTP, and liberates the G protein βγ subunits (Ste4/Ste18). Sustained signaling requires activation of multiple effectors (not shown) by the dissociated Gβγ components. These effectors activate a pathway (*dotted line*) leading to transcription of several genes including the RGS protein (Sst2). GTP hydrolysis is accelerated by the RGS protein, and this leads to subunit reassociation and pathway inactivation. The model assumes that GTP hydrolysis is the rate-limiting step of subunit reassembly. A potential positive feedback loop leading to Sst2 degradation is indicated by a *darker line*. *B*, in the computer simulation the concentration of free Gβγ (*solid line*) increases rapidly after addition of pheromone (at time = 0). The concentration of RGS (*dashed line*) responds slowly and eventually inactivates the pathway leading to a reduction in free Gβγ. The experimentally observed induction of Sst2 (from Fig. 1*B*) is also shown (*solid circles*). The details of the model and parameter values used in the computer simulation are presented under "Experimental Procedures."

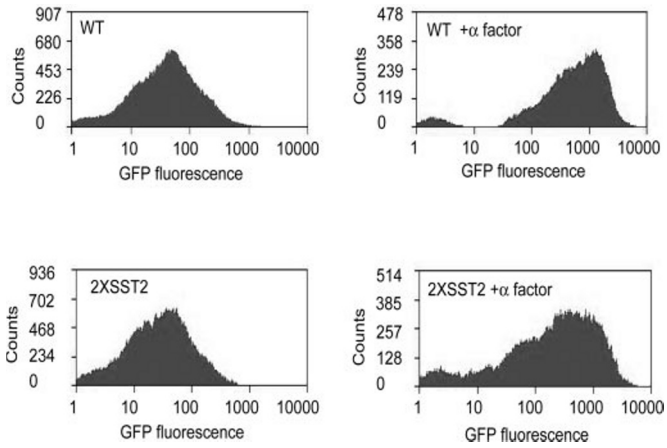

FIG. 5. **Double expression of Sst2 eliminates the response in a subpopulation of cells.** Pheromone-dependent transcriptional induction was measured following transformation of wild-type cells with a single copy plasmid (pRS316) containing genomic *SST2* (2xSST2) or transformation of wild-type cells with the same plasmid containing no insert (*WT*). The same cells were co-transformed with a pheromone-responsive *FUS1* promoter-GFP reporter. Cells were then treated with α-factor for 90 min, and the resulting fluorescence in each cell was monitored by cell sorting. Pathway activation results in an increase in cells with >100 fluorescence units of activity. The peak below 10 units is also seen in cells lacking the reporter and likely represents autofluorescence noise.

where R_{min} is the response in the absence of pheromone, and R_{max} is the maximum response. Explicit expressions for R_{min}, R_{max}, and C in terms of $[L]$, steady-state RGS concentration, and the model parameters are provided under "Experimental Procedures." As can be seen from Fig. 2*C*, the model correctly captures the increased response over the entire range of pheromone concentration where Gβ is overexpressed (Fig. 2*B*). The model also captures the dependence of the EC_{50} on Sst2 (compare Fig. 3, *A* and *B*).

There are two qualitative features of the data that are not captured by the model. First, deletion of *SST2* had no affect on the maximum response, whereas 2-fold overexpression of *SST2* produced a 27% reduction in the maximum response (Fig. 3*A*). The model cannot simultaneously account for both observations. Second, in the strain containing two copies of *SST2* the expression level was relatively constant at early times following pheromone addition and then increased sharply between 60 and 105 min (Fig. 1*B*). The initial slow increase in Sst2 expression followed by a rapid increase in expression is not consistent with the model.

To investigate the discrepancies between the experimental results and the model predictions, the transcription assay was repeated using the green fluorescent protein (GFP) instead of β-galactosidase as a reporter. The use of GFP allows the activity of *individual cells* to be measured by flow cytometry (20, 23). Wild-type cells containing a single copy plasmid containing no insert or a genomic *SST2* clone (2xSST2) were treated with α-factor for 90 min. As shown in Fig. 5 there is in all cells a single peak of low intensity fluorescence (peak activity between 10 and 100 units) in the absence of pheromone, which upon pheromone treatment is diminished and replaced by a second peak of higher intensity (peak activity between 100 and 1000 units) (23). Whereas the shift from low intensity to high intensity was nearly complete under normal conditions, a prominent low intensity peak persisted in cells that overexpress *SST2*. These data indicate that the reduced maximum response seen in Fig. 3*A* is most likely due to a subpopulation of cells that is completely unresponsive. Whereas the response to pheromone is normally graded, it can become binary (all-or-none) when Sst2 is overexpressed.

One way that binary responses can occur is through positive feedback regulation (31). Thus we considered a phenomenological model in which pheromone promotes a second feedback loop leading to faster Sst2 *degradation* (see "Experimental Procedures" for details of the model). The model makes the reasonable assumption that alterations in the expression of Sst2 occur more slowly than alterations in the activation state of the G protein. Stated differently, the activation state of the G protein adjusts rapidly to the slow variation in Sst2 concentration and is therefore assumed to be in equilibrium. This assumption allows the state of the system to be determined by Sst2 expression levels alone. The model for the 2xSST2 strain is shown schematically in Fig. 6*A*. The rates of Sst2 production (*solid lines*) and degradation (*dashed lines*) are shown as a function of Sst2 expression. The *two straight lines* represent Sst2 production and degradation rates in the absence of pheromone. In this case production was independent of Sst2 expression, while degradation was proportional to Sst2 expression.

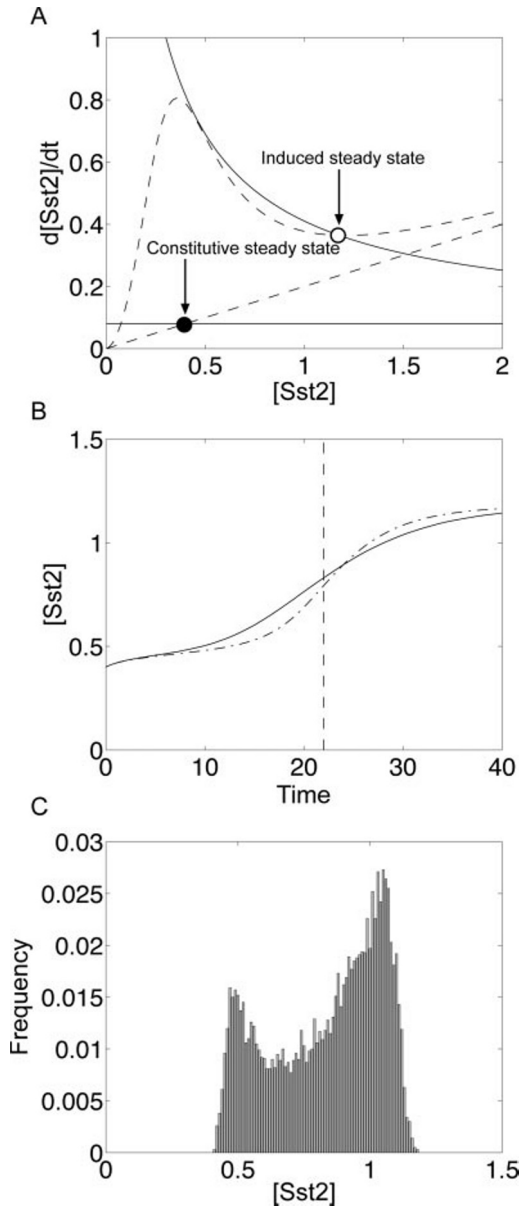

FIG. 6. **Modeling Sst2 inhibition.** *A*, Sst2 production rates (*solid lines*) and degradation rates (*dashed lines*) as a function of Sst2 concentration. The *two straight lines* are the constitutive rates. Where the lines intersect represents a steady state (*Constitutive steady state*). The *upper curves* are the pheromone-induced rates. At moderate Sst2 levels, pheromone-induced expression and degradation are enhanced and almost equal causing the system to respond slowly. At high Sst2 levels the pathway is inhibited, so transcription and degradation of Sst2 are also diminished and eventually reach a new steady state (*Induced steady state*). *B*, time courses generated by the model depicted in *A*. The slow response of the system at early times is clearly visible. The *solid line* is the result from the model in the absence of stochastic effects. The *dot-dashed line* is the average result for the stochastic model. Details of the model and parameter values are given under "Experimental Procedures." *C*, a histogram of the data generated by the stochastic model of Sst2 inhibition. The *dashed vertical line* indicates the time at which samples were collected and clearly shows a binary response that is transient and disappears at later times. Values for Sst2 concentration and times are arbitrary.

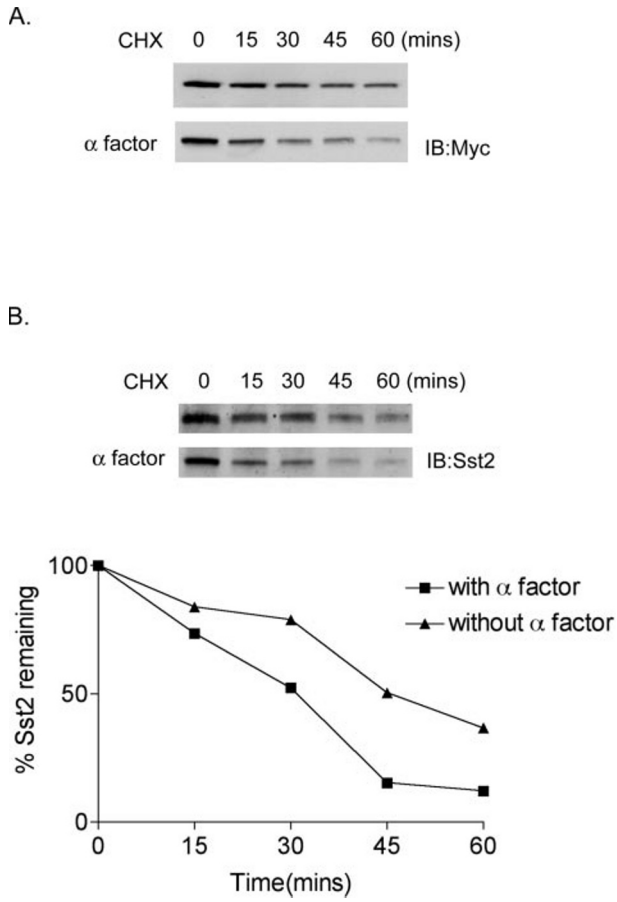

FIG. 7. **Pheromone stimulation promotes the degradation of Sst2.** An *sst2*Δ mutant strain transformed with a single copy plasmid (pRS315-ADH) containing *SST2* under the control of a constitutive promoter (from *ADH1*) (*A*) or wild-type cells expressing genomic *SST2* and the native promoter (pRS315) (*B*) were treated with 3 μM α-factor for 60 min and then treated with the protein synthesis inhibitor cycloheximide (*CHX*) for the indicated times. Cell extracts were analyzed by immunoblotting with anti-Sst2 antibodies as described in Fig. 1. To estimate the difference in protein half-life the intensity of each band was analyzed by densitometric scanning. The data are representative of one (*A*) or two (*B*) independent experiments. *IB*, immunoblot.

Where the lines intersect production and degradation rates are equal ("constitutive steady state"). The *two curved lines* represent Sst2 production and degradation rates in the presence of pheromone. At low Sst2 expression, the induced production rate exceeded the constitutive production rate. At higher Sst2 expression the pathway was inhibited, *SST2* transcription was diminished, and the induced production rate approached the constitutive rate. The degradation rate also had a non-linear dependence on Sst2 expression. At low Sst2 expression, pheromone promoted Sst2 degradation as part of a positive feedback mechanism. At higher Sst2 expression the pathway was inhibited, Sst2 degradation was diminished, and the induced degradation rate approached the constitutive rate. Where the lines intersect production and degradation rates are equal ("induced steady state").

Using the revised model we can understand the slow initial induction of Sst2 seen for the 2xSST2 strain (see Fig. 1*B*). Initially the system is in steady state ([Sst2] ~ 0.4). After exposing the cells to α-factor, the production rate exceeds the degradation rate slightly, and the Sst2 levels slowly increase. As Sst2 expression increases the degradation rate falls more rapidly than the production rate, and eventually the level of Sst2 begins to rise until it reaches a new steady state ([Sst2] ~ 1.2). The *dot-dashed line* in Fig. 6*B* is a time series produced by this model and shows good qualitative agreement with the experimental results in Fig. 1*B*. For simulation of the 2xSST2 strain, the constitutive and pheromone-induced production rates were double that of the wild-type strain.

In the model described above, even for the 2xSST2 strain, there is only one steady state. To test whether this model can reproduce the binary response seen in the single cell transcrip-

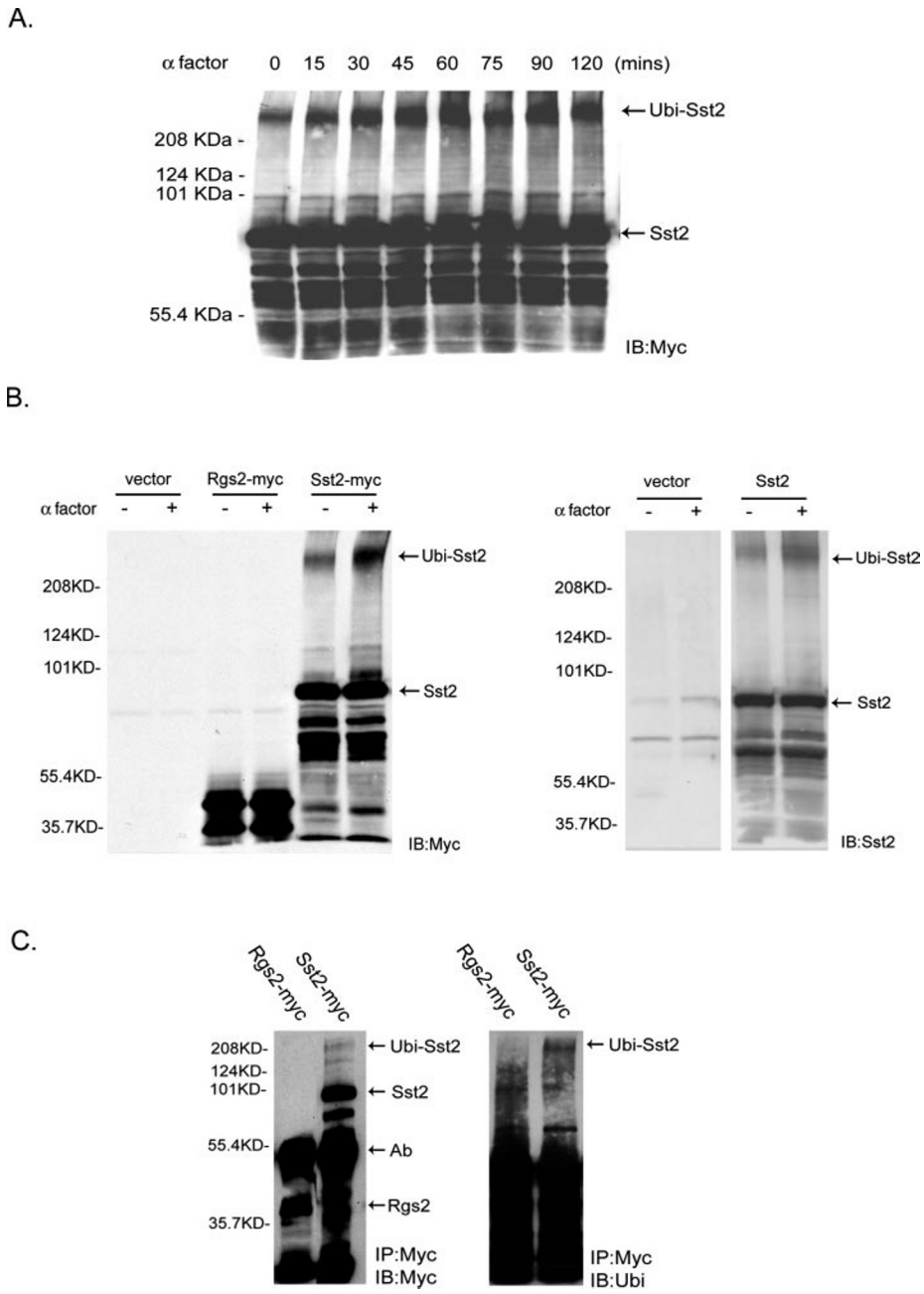

FIG. 8. **Pheromone promotes the ubiquitination of Sst2.** *A*, wild-type cells were transformed with pRS316-ADH-SST2-myc and treated with 3 μM α-factor for the indicated times. Whole-cell lysates were then prepared and resolved by 7.5% SDS-PAGE and immunoblotting. Monoclonal anti-Myc antibodies detected the Myc epitope-tagged Sst2-myc (*Sst2*) and a broad high molecular weight species corresponding to a likely ubiquitinated form of Sst2 (*Ubi-Sst2*) that accumulated over time. *B*, to confirm that the high molecular weight species is in fact Sst2, wild-type cells were transformed with the Myc-tagged form of Sst2 and probed with anti-Myc monoclonal antibodies. The high molecular weight species was recognized by the anti-Myc antibody, accumulated with pheromone treatment, and was absent in the control cells transformed with an empty vector or another Myc-tagged protein (Rgs2) (*left panel*). The Sst2 species detected with the Myc antibodies was also detected using the anti-Sst2 antibodies (*right panel*). *C*, to confirm ubiquitination of Sst2 the same cells were immunoprecipitated with anti-Myc antibodies (*IP*), resolved by 7.5% SDS-PAGE and immunoblotting, and probed with anti-ubiquitin antibodies (*IB*). Data are representative of at least two independent experiments. *IB*, immunoblot; *Ubi*, ubiquitin.

tion assay shown in Fig. 5 we added a stochastic term to the model to account for random fluctuations in protein concentrations levels. We then performed 10,000 simulations of the random model and averaged the results to yield the mean time course indicated by the *solid line* in Fig. 6*B*. Fig. 6*C* is a histogram of the modeled Sst2 concentrations for each simulation at single time points indicated by the *vertical line* at time ~ 22 (Fig. 6*B*). The results presented in Fig. 6*C* show a clear binary response similar to that observed for the 2xSST2 strain (Fig. 5).

Taken together, the revised model requires the existence of a positive feedback mechanism leading to pheromone-dependent loss of Sst2. Thus we investigated whether pheromone treatment does in fact promote the degradation of Sst2. After 1 h of growth in the absence or presence of pheromone the cells were treated with cycloheximide to block new protein synthesis. Steady-state levels of Sst2 remaining were then monitored by immunoblotting. As shown in Fig. 7, Sst2 abundance declined more quickly when pretreated with pheromone. A similar pattern of degradation was observed when *SST2* was expressed from a constitutive promoter (Fig. 7*A*) or the native promoter (Fig. 7*B*). These data indicate that pheromone stimulates the degradation of Sst2 as predicted by the model.

We then investigated whether pheromone-dependent Sst2 degradation results from ubiquitination, a modification that has been reported for some mammalian RGS proteins (32, 33). Ubiquitination is the formation of an isopeptide bond between the ubiquitin polypeptide and Lys side chains of the target protein (34). Ubiquitin is itself ubiquitinated, resulting in the formation of polyubiquitin chains. The polyubiquitinated protein is usually then captured and degraded by a large protease complex, the 26 S proteasome (35). To determine whether Sst2 is ubiquitinated we analyzed the expression of a Myc epitope-tagged version of the protein. As shown in Fig. 8*A*, long exposures of Sst2-myc immunoblots revealed a very high molecular weight immunoreactive band, suggesting that the protein is indeed polyubiquitinated. This high molecular weight species was barely visible in the untreated cells but accumulated with

time and became fully modified after 60 min of pheromone treatment. To confirm that the high molecular weight band is Sst2 we demonstrated that it is recognized by anti-Sst2 as well as anti-Myc antibodies (Fig. 8*B*). As an additional control we constructed a Myc-tagged version of a second RGS protein in yeast, Rgs2. Rgs2 regulates Gpa2 specifically, having no effect on the Gpa1-mediated pheromone response (36). As shown in Fig. 8*B*, Rgs2 did not exhibit any change in mobility either in the absence or presence of pheromone. To confirm that the appearance of a high molecular weight form of Sst2 is due to ubiquitination, the protein was immunoprecipitated with anti-Myc antibodies and analyzed by immunoblotting with anti-ubiquitin antibodies. This enrichment scheme again yielded a high molecular weight band recognized by both anti-ubiquitin and anti-Myc antibodies (Fig. 8*C*).

The data presented above indicate that pheromone promotes the ubiquitination and degradation of Sst2. To determine whether ubiquitination of Sst2 leads to degradation, we searched for mutants that diminish Sst2 ubiquitination and investigated their effects on Sst2 turnover. Ubiquitination typically requires three distinct enzymatic activities: a ubiquitin-activating enzyme (E1), a ubiquitin-conjugating enzyme (E2), and a ubiquitin ligase (E3). For our experiments we tested strains lacking E2 ubiquitin-conjugating enzymes since most E2-encoding enzymes are not essential, and their identity is more clearly defined than the E3 enzymes. All available E2-deficient deletion mutants were treated with pheromone for 1 h and then analyzed by immunoblotting with anti-Sst2 antibodies. As shown in Fig. 9*A*, Sst2 ubiquitination was diminished in the E2 mutant *ubc2*Δ but was preserved in all the other mutant and wild-type strains tested.

We then compared the turnover rate of Sst2 in *ubc2*Δ mutant and wild-type cells both in the absence and presence of pheromone. Cells in mid-log phase were treated with cycloheximide to block new protein synthesis and analyzed by immunoblotting with anti-Myc antibodies. As shown in Fig. 9*B* the overall level of Sst2 dropped rapidly when translation was blocked in wild-type cells, while the half-life was extended dramatically in the *ubc2*Δ mutant. We conclude from these results that Sst2 degradation is slowed when it is no longer ubiquitinated. Taken together, our findings indicate that pheromone promotes not only the transcription of *SST2* but also the ubiquitination and subsequent degradation of the protein. Together these mechanisms could account for the transient expression of the protein following pheromone challenge.

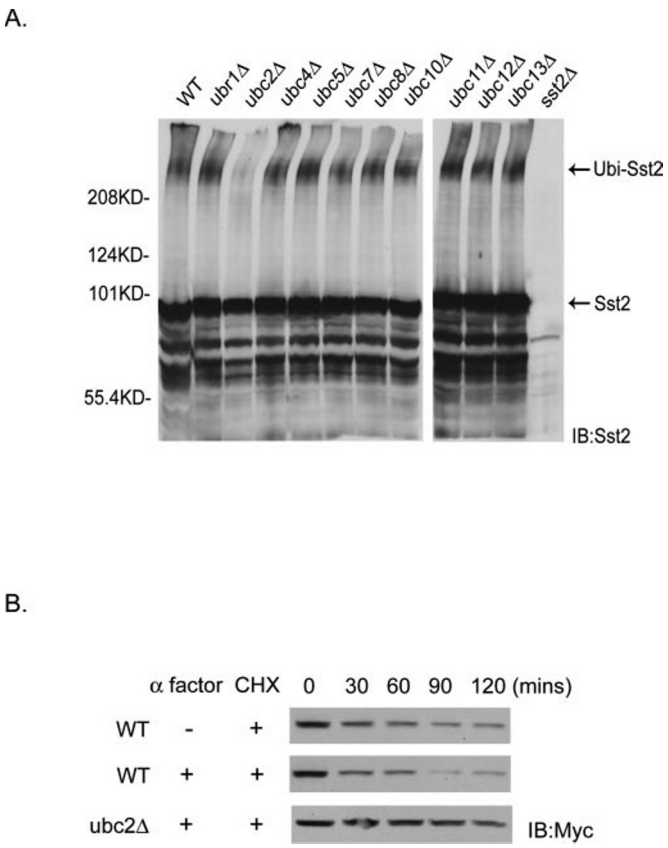

FIG. 9. **Ubiquitination of Sst2 promotes degradation.** *A*, wild-type strains or isogenic mutant strains lacking the indicated gene were transformed with pAD4M-SST2 and treated with 3 μM α-factor for 60 min. Cell extracts were analyzed by immunoblotting with anti-Sst2 antibodies. Of the strains tested, only *ubc2*Δ mutants exhibited diminished ubiquitination of Sst2. *B*, to determine whether diminished ubiquitination results in diminished degradation, wild-type and *ubc2*Δ cells were transformed with pRS316-ADH-SST2-myc. Cells were treated with 3 μM α-factor and cycloheximide as indicated. Cell extracts were then resolved by SDS-PAGE and immunoblotting with anti-Myc antibodies to detect Sst2 remaining. Data are representative of at least two independent experiments. *Ubi*, ubiquitin; *IB*, immunoblot; *WT*, wild type; *CHX*, cycloheximide.

DISCUSSION

Biologists have traditionally described the cellular functions of proteins in qualitative terms with models based largely on intuition. Such models typically ignored temporal aspects of protein activity and therefore failed to predict behavior resulting from changes in protein expression and turnover. Moreover, while cellular metabolic or signaling pathways were once described as linear and unidirectional, they are now recognized to consist of complex networks subject to positive and negative feedback regulation. As our understanding of these pathways becomes more sophisticated, however, it has become possible to devise models that can account for their complex behaviors and are therefore more accurate, comprehensive, and quantitative. Our ability to identify genes, manipulate their expression, and quantify their function has also improved to the point where computation models can be reasonably tested experimentally.

Here we devised a quantitative model that considers the activation, desensitization, and resensitization steps following pheromone stimulation in yeast. This approach allowed us to demonstrate the importance of negative feedback inhibition through induction of RGS expression (desensitization) and also prompted our discovery of a positive feedback loop leading to RGS ubiquitination and degradation (resensitization). Only by taking into account this second feedback loop were we able to adequately explain the available functional data.

The existence of both positive and negative controls on RGS protein expression, acting in sequence, could serve as a timing mechanism to allow multiple rounds of pathway activation. If G protein activation occurred without RGS induction the system would reach a stable and non-productive "on" state. Conversely RGS degradation may be required to eventually restore pheromone responsiveness in haploid cells, thereby increasing the prospect of a second chance at successful conjugation.

Sst2 joins a small but growing list of signaling proteins that undergo ubiquitination. In the pheromone response pathway, receptors (37–39), the Gα subunit (40, 41), and the effector kinase Ste7 (42, 43) are known substrates for ubiquitination. Ubiquitination of Ste7 is dependent on prolonged pheromone stimulation, and once ubiquitinated it is rapidly degraded by the proteasome (42, 43). Ubiquitination of the receptor is also accelerated by pheromone. However, this situation is unusual in that the receptor is monoubiquitinated rather than polyubiquitinated, and ubiquitination in this case serves as a signal for endocytosis and delivery to the vacuole instead of the proteasome (37–39). Ubiquitination of the G protein is not regulated by pheromone but is noteworthy because it was the first

ubiquitination site to be directly mapped by mass spectrometry (41).

Biologists and applied mathematicians have long used similar methods to describe input-output relationships of complex systems. The dose-response profiles so familiar to biologists are equally well known to theorists, who refer to them as one-parameter bifurcation diagrams (31). Dose-response profiles are used by pharmacologists and physiologists to predict the response of a cell to a specific dose of drug or hormone. Such profiles are also useful to theorists because they summarize the general, qualitative properties of solutions of a set of non-linear differential equations. However, because theorists are not constrained by the same technical and ethical considerations that preclude certain biological experiments they may be able to describe or interpret cellular behavior in ways that experimentalists cannot and therefore have the potential to greatly enrich our understanding of biological systems. An example of this potential was realized here in our ability to devise a model of response regulation by Sst2. While the model did not explicitly account for every biochemical step in the pathway, it was consistent with the known biology of G protein signaling. An advantage of using this simple model was that it allowed us to make several predictions that could be compared with experimental data. In particular, we found that the model could not simultaneously account for the behavior of the 2xSST2 strain, the *sst2*Δ mutant, and the wild-type strain at saturating pheromone levels. The model could also not reproduce the slow induction of Sst2 expression observed for the 2xSST2 strain. The inconsistencies prompted further experiments, which in turn led to a revised model.

In summary, our analysis accounts for three key aspects of G protein-mediated signaling. The signal initiation step, already well established, requires receptor-catalyzed guanine nucleotide exchange. The second step consists of a negative feedback loop by which pheromone promotes RGS expression and G protein inactivation. RGS proteins were already well known to inhibit signaling, but the contribution of transcriptional induction had not previously been demonstrated. The third step was previously unknown and invokes a positive feedback mechanism through induction of RGS protein ubiquitination and degradation. These findings illustrate how computational modeling, which is not by itself hypothesis-driven, can generate a novel hypothesis about protein function that can be tested experimentally.

Having described the activity of the early steps in the pheromone signaling pathway, our present goal is to model activation of downstream effectors and eventually create computer simulations of the entire pathway. This should be feasible given that there are relatively few components, and their activities are well understood. Such studies should provide new insights about how cells communicate and respond to external stimuli and how those responses change over time. The combination of experimental and computational approaches used here could also be applied to other signaling pathways and other organisms and promises to improve our understanding of how cellular changes in disease states can be predicted and managed.

Acknowledgments—We are grateful to Lorena Kallal, Mark Hall, and Daria Siekhaus for generously providing plasmids and expert advice; Duane Jenness and James Konopka for antibodies; and Jason Snyder for purified Gpa1.

REFERENCES

1. Bhalla, U. S., Ram, P. T., and Iyengar, R. (2002) *Science* **297,** 1018–1023
2. Riccobene, T. A., Omann, G. M., and Linderman, J. J. (1999) *J. Theor. Biol.* **200,** 207–222
3. Shea, L. D., Neubig, R. R., and Linderman, J. J. (2000) *Life Sci.* **68,** 647–658
4. Ferrell, J. E., Jr., and Machleder, E. M. (1998) *Science* **280,** 895–898
5. Bhalla, U. S., and Iyengar, R. (1999) *Science* **283,** 381–387
6. Dohlman, H. G., and Thorner, J. W. (2001) *Annu. Rev. Biochem.* **70,** 703–754
7. Guo, M., Aston, C., Burchett, S. A., Dyke, C., Fields, S., Rajarao, S. J. R., Uetz, P., Young, K., and Dohlman, H. G. (2003) *Mol. Cell* **12,** 517–524
8. Dohlman, H. G. (2002) *Annu. Rev. Physiol.* **64,** 129–152
9. Neves, S. R., Ram, P. T., and Iyengar, R. (2002) *Science* **296,** 1636–1639
10. Dohlman, H. G., Apaniesk, D., Chen, Y., Song, J., and Nusskern, D. (1995) *Mol. Cell. Biol.* **15,** 3635–3643
11. DiBello, P. R., Garrison, T. R., Apanovitch, D. M., Hoffman, G., Shuey, D. J., Mason, K., Cockett, M. I., and Dohlman, H. G. (1998) *J. Biol. Chem.* **273,** 5780–5784
12. Dohlman, H. G., Song, J., Ma, D., Courchesne, W. E., and Thorner, J. (1996) *Mol. Cell. Biol.* **16,** 5194–5209
13. Apanovitch, D. M., Slep, K. C., Sigler, P. B., and Dohlman, H. G. (1998) *Biochemistry* **37,** 4815–4822
14. Chan, R. K., and Otte, C. A. (1982) *Mol. Cell. Biol.* **2,** 21–29
15. Chan, R. K., and Otte, C. A. (1982) *Mol. Cell. Biol.* **2,** 11–20
16. Shea, L., and Linderman, J. J. (1997) *Biochem. Pharmacol.* **53,** 519–530
17. Ausubel, F. M., Brent, R., Kingston, R. E., Moore, D. D., Seidman, J. G., Smith, J. A., and Struhl, K. (eds) (1987) *Current Protocols in Molecular Biology*, Wiley-Interscience, New York
18. Sikorski, R. S., and Hieter, P. (1989) *Genetics* **122,** 19–27
19. Song, J., Hirschman, J., Gunn, K., and Dohlman, H. G. (1996) *J. Biol. Chem.* **271,** 20273–20283
20. Siekhaus, D. E., and Drubin, D. G. (2003) *Nat. Cell Biol.* **5,** 231–235
21. Kallal, L., and Fishel, R. (2000) *Yeast* **16,** 387–400
22. Hoffman, G., Garrison, T. R., and Dohlman, H. G. (2002) *Methods Enzymol.* **344,** 617–631
23. Poritz, M. A., Malmstrom, S., Kim, M. K., Rossmeissl, P. J., and Kamb, A. (2001) *Yeast* **18,** 1331–1338
24. Dohlman, H. G., Goldsmith, P., Spiegel, A. M., and Thorner, J. (1993) *Proc. Natl. Acad. Sci. U. S. A.* **90,** 9688–9692
25. Evan, G. I., Lewis, G. K., Ramsay, G., and Bishop, J. M. (1985) *Mol. Cell. Biol.* **5,** 3610–3616
26. Kepler, T. B., and Elston, T. C. (2001) *Biophys. J.* **81,** 3116–3136
27. Jenness, D. D., Burkholder, A. C., and Hartwell, L. H. (1986) *Mol. Cell. Biol.* **6,** 318–320
28. Cole, G. M., and Reed, S. I. (1991) *Cell* **64,** 703–716
29. Janetopoulos, C., Jin, T., and Devreotes, P. (2001) *Science* **291,** 2408–2411
30. Whiteway, M., Hougan, L., and Thomas, D. Y. (1990) *Mol. Cell. Biol.* **10,** 217–222
31. Tyson, J. J., Chen, K. C., and Novak, B. (2003) *Curr. Opin. Cell Biol.* **15,** 221–231
32. Davydov, I. V., and Varshavsky, A. (2000) *J. Biol. Chem.* **275,** 22931–22941
33. Kim, E., Arnould, T., Sellin, L., Benzing, T., Comella, N., Kocher, O., Tsiokas, L., Sukhatme, V. P., and Walz, G. (1999) *Proc. Natl. Acad. Sci. U. S. A.* **96,** 6371–6376
34. Pickart, C. M. (2001) *Annu. Rev. Biochem.* **70,** 503–533
35. Voges, D., Zwickl, P., and Baumeister, W. (1999) *Annu. Rev. Biochem.* **68,** 1015–1068
36. Versele, M., de Winde, J. H., and Thevelein, J. M. (1999) *EMBO J.* **18,** 5577–5591
37. Hicke, L., and Riezman, H. (1996) *Cell* **84,** 277–287
38. Hicke, L., Zanolari, B., and Riezman, H. (1998) *J. Cell Biol.* **141,** 349–358
39. Roth, A. F., Sullivan, D. M., and Davis, N. G. (1998) *J. Cell Biol.* **142,** 949–961
40. Madura, K., and Varshavsky, A. (1994) *Science* **265,** 1454–1458
41. Marotti, L. A., Jr., Newitt, R., Wang, Y., Aebersold, R., and Dohlman, H. G. (2002) *Biochemistry* **41,** 5067–5074
42. Wang, Y., and Dohlman, H. G. (2002) *J. Biol. Chem.* **277,** 15766–15772
43. Wang, Y., Ge, Q., Houston, D., Thorner, J., Errede, B., and Dohlman, H. G. (2003) *J. Biol. Chem.* **278,** 22284–22289
44. Stone, D. E., Cole, G. M., de Barros Lopes, M., Goebl, M., and Reed, S. I. (1991) *Genes Dev.* **5,** 1969–1981